Proceedings of ALGORITMY 2012
pp. 353–361

BRIDGING LAW SHAPE FOR LONG FIBRE COMPOSITES AND ITS FINITE ELEMENT CONSTRUCTION*

VLADISLAV KOZÁK † AND ZDENEK CHLUP‡

Abstract. Ceramic matrix composites reinforced by unidirectional long fibres are very perspective materials. Especially glass matrix composites reinforced by unidirectional long ceramic fibres are very complicated materials for modelling thanks their common acting of various micromechanisms like pull out, crack bridging, matrix cracking etc. Crack extension is simulated by means of element extinction algorithms. The principal effort is concentrated on the application of the cohesive zone model with the special traction separation law (bridging). Determination of micro-mechanical parameters is based on the combination of static tests, microscopic observation and numerical calibration procedures. The paper is oriented to the construction of the new type of element for FEM program (Abaqus).

Key words. finite element method, cohesive elements, bridging law

AMS subject classifications. 74S05, 74E30, 74E20

1. Introduction. Crack growth modelling achieved during last decade great success and progress. The finite element and boundary element method, molecular dynamic success and actually "ab initio" computation found their use in the material research long time ago. Some of mentioned methods are modified, e.g. parallel approach implementation, which comes into their own in case of the multiprocessor applications. In some cases only the small improvement of the standard procedures is coming. The finite element method as a well known procedure has in this case the special position. It seemed that the boundary of material and geometry nonlinearities will be reached later. Procedures based on the fracture mechanics approach derived benefit from knowledge of global parameters like the stress intensity factor and J integral are. These parameters were used with the combination of the remeshing ahead the crack tip a bit later.

The special element implementation responding damage and crack growth introduced so-called "damage mechanics". The cohesive elements are similar; the origin can be found in the contact elements and is based on the vanishing elements and the new surface creation [1]. The phenomenological description characterizing material behaviour is realized using the traction-separation law, thanks this the local damage is predicted. Many models published within last five years can be found in literature for laminates, composites, long fibre composites etc.

Although the cohesive zone modelling is used more than one decade, the physical interpretation of the cohesive zone is still discussed. This zone has practically zero thickness which can be in contradiction of the classical fracture mechanic approach. Characteristics of the physical cohesive zones peak traction, critical separation, work of separation $(T_0, \delta_0, \Gamma_0)$ can be derived by the strain and stress analysis in narrow bands [2]. Since the cohesive model is a phenomenological model, there is no evidence,

*This work was supported by Grant No.: P107/12/2445 of the Grant Agency of the Czech Republic.

†Institute of Physics of Materials AS of CR, Brno Czech Republic (kozak@ipm.cz).

‡Institute of Physics of Materials AS of CR, Brno Czech Republic

which form is to be taken for the cohesive law. Thus cohesive law has to be assumed independently of specific material as a model of the separation process. Most authors take their own formulation for the dependence of the traction on the separation. The exponential model is used by many authors for both the ductile and the cleavage fracture. The $T-\delta$ response follows an irreversible path with unloading always direct to origin. This model represents all the features of the separation process by: (1) the shape of the cohesive traction-separation curve $T-\delta$, (2) the local material strength by the peak traction T_0, and the work of separation Γ_0 given by the area under $T-\delta$ curve.

Cohesive model use is realized by two types of elements. The first one is described by the classical continuum; the second one is the linking cohesive element. The separation of the cohesive element is computed from the displacement of the standard element. In general terms the separation is dependent on the normal and shear stress constituent and their operation on the linking element [3], [4]. Composite damage modelling on the base of knowledge of crucial micromechanisms is one of the good approaches how to ensure compliance to the prediction and experiment. When the crack is propagates in the composite in the direction perpendicular to the strengthen fibres, the damage is then determined by these basic micromechanisms: matrix cracking, delamination of an interface fibre and matrix, fibre cracking, fibre pull out [5]. The critical problem is to predict interface behaviour between the fibre and the matrix. This interaction plays crucial role in the determination of the final fracture toughness, fracture strength and the general fracture behaviour.

¿From the micromechanical point a view, every element has its own microstructure, it comes out from the representative volume element (RVE) approach and the material separation and damage is described and determined by the cohesive element. In this manner we separate material behaviour into two distinctively different areas. Crack propagation through the element is described by the fracture mechanic and by the cohesive model. This model is simpler than the classical models and is parameters are determined experimentally [6], [7], [8]. The cohesive models are widely used in case of the crack growth and fragmentation simulation for metals, polymers and ceramics [8], [9].

Outstanding progress in the crack growth modelling has been achieved by onset of the extended finite element method (X-FEM) in the last years. This method seems be very perspective, no remeshing is used and crack growth goes through the element. By this way one can avoid various numerical problems which is necessary to solve by using the connection elements of interface type [10], [11]. Last innovation for the crack growth modelling without remeshing is the combination of the extended finite element method and application of the cohesive law as a controlling procedure for the crack growth modelling.

2. Traction-separation law. For a general constitutive modelling of materials whose fracture may be described by means of a cohesive crack, we need to define three main ingredients: (1) The stress-strain behaviour of the material in absence of cohesive cracks, as described by classical constitutive modelling. (2) The initiation criterion, which determines the conditions in which a crack will form and the orientation of the newly formed cohesive crack. (3) The evolution law for the cohesive crack, which relates the stresses transferred between its faces to the relative displacement between the crack lips.

The cohesive crack model may serve to predict structural behaviour or to analyze

experimental results. However, it can also be used to analyze certain wider aspects of material or structural behaviour. This requires, in general, a certain type of specialization: the type of softening curves and the range of sizes or geometries must be selected and then a systematic analysis carried out from which general conclusions can be drawn about the aspects that have been studied. In the particular model the cohesive elements are surrounded by the classical elements. When the cohesive elements are damaged the crack is extended over the boundaries of the classical elements. In general, the crack is propagated only in areas where the cohesive elements are inserted and the crack growth direction is predicted before the numerical computation.

In common for all cohesive laws: (a) comprises two material parameters δ_0, T_0, (b) after the material damage the stress becomes zero, $T(\delta > \delta_0) = 0$, for normal and tangential separation (this condition is not exactly fulfilled for all cohesive laws). The area below the traction-separation curve whether for tangential or for normal direction gives us the energy dissipated by the cohesive element Γ_0. A schematic diagram for the long fibre composite can be seen in Fig. 2.1. A leading edge up to maximal stress looks like Dirac function; it is clear that from the numerical point a view this shape of the traction-separation law is the source of instabilities and the numerical solution probably is going to diverge. It is necessary this singularity smooth away for $\Delta u = 0$, respectively introduce the strength J_0.

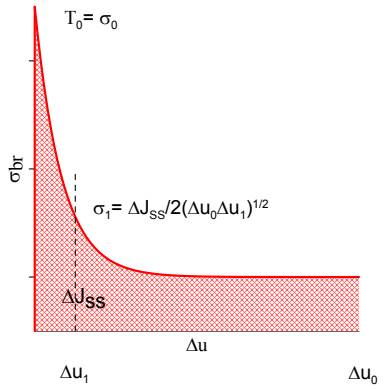

FIG. 2.1. *A shape of the bridging law for long fibre composite.*

3. Bridging law and FE modelling. Let us think over a body having crack perpendicular to the direction of oriented fibres. If we found a relation between the bridging stress σ_{br} and fracture energy, then by means of fracture mechanics one can predict crack growth and propagation. The bridging law in the form of $\sigma = \sigma(\delta)$ is identical in every point of bridging zone. In case of shock loading the damage of fibres comes straightaway, therefore is inevitable to suppose an existence of characterizing opening δ_0, which determines the moment when the bridging effect is vanishing. Contrary of the crack resistance curve (R curve or $J - \Delta$ curve) the bridging law is accepted such as the material characteristic. Fracture energy splitting by means of J integral on the crack surface and the crack vicinity gives:

$$J = \int_0^{\delta^*} \sigma(\delta) d\delta + J_{TIP}, \tag{3.1}$$

where J_{TIP} is the J integral evaluated around the crack tip (during cracking is equal to the fracture energy of the tip, J_0). The total energy is then dissipated in the bringing zone and δ^* is the maximum opening of the bridging zone at the notch root. The bridging law can be determined by differentiating Eq. 3.1:

$$\sigma(\delta^*) = \frac{\partial J_R}{\partial \delta}, \tag{3.2}$$

J_R is the value of J integral during the crack growth. Initially the crack is without the bridging stress and the initiations starts when $J_R = J_{TIP} = J_0$. Special shapes of the bridging law can be found in [12]. The shape of the bridging law can be described by Eq. 3.3, it seems to be very suitable for the long fibre composites. When the end opening of the bridging zone reaches δ_0 the steady state value of fracture energy is reached, see Fig. 3.1,

$$J_R(\delta^*) = J_0 + \Delta J_{SS}(\frac{\delta^*}{\delta_0})^{1/2}. \tag{3.3}$$

They are many shapes of the cohesive laws and many ways how to implement this law in the commercial standard FEM package. The authors come out from the long-standing knowledge of Abaqus system, where the user procedure UEL enables very effectively implement the new element into this package and eventually to change the shape of the bridging law. The function in Eq. 3.4 is declared in literature [12] and [13] as a very convenient for the application on the long fibre composites

$$\sigma_{br}(\delta) = \frac{\Delta J_{SS}}{2\delta_0}(\frac{\delta}{\delta_0})^{-1/2}. \tag{3.4}$$

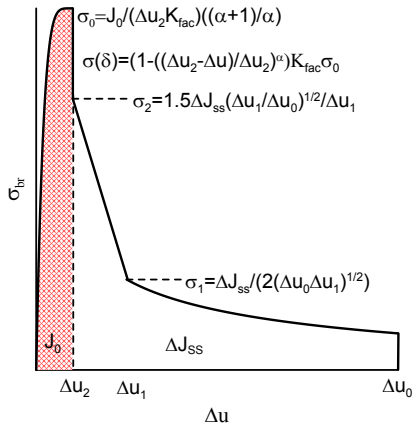

FIG. 3.1. *Optimized shape of the bridging law.*

The Fig. 3.1 shows the optimized shape of the cohesive law, a leading edge in the chart plays important role for the numerical stability of the interface element. The element is made up of two quadratic line elements for 2D plane elements or two quadratic plane elements for 3D. The node numbering is chosen according to numbering according to Abaqus conventions. Two surfaces of the interface element initially lie together in initial stage; it is in the unstressed deformation state. The relative

displacements of the element faces create normal and shear displacements depending on the constitutive equation. Now we suppose the quadratic line element for 2D simulations. This element has 12 degrees of freedom and the nodal displacement vector is given by Eq. 3.5

$$\boldsymbol{d}_N = (d_x^1, d_y^1, d_x^2, d_y^2, ...d_x^6, d_y^6). \tag{3.5}$$

The plane interface element (for 3D) has 48 (3x16) degrees of freedom. The elements ordering follows from the standard conventions, then the opening of the connection element is determined as a difference in displacements between the top (TOP) and bottom (BOT) nodes:

$$\Delta u = u^{TOP} - u^{BOT}. \tag{3.6}$$

Then we can define the interface opening in terms of nodal displacements of paired nodes:

$$\Delta \boldsymbol{u}_N = \Phi \boldsymbol{d}_N = [-I_{6x6} \mid I_{6x6}] \boldsymbol{d}_N. \tag{3.7}$$

where I_{6x6} is unity matrix with 6 rows and columns, $\boldsymbol{u}_N$ is a 6x1 vector. From the nodal positions the crack opening is interpolated to the integration points with the help of standard shape functions. Let $N_i(\xi)$ be the shape function for node pair i (i = 1,2,3), where ξ stands position in the local coordinate system $-1 < \xi < 1$. The relative displacement between the nodes within the elements is then given:

$$\Delta \boldsymbol{u}(\xi) = \begin{pmatrix} \Delta u_x(\xi) \\ \Delta u_y(\xi) \end{pmatrix} = H(\xi) \Delta \boldsymbol{u}_N, \tag{3.8}$$

where $H(\xi)$ is matrix 2x6 containing the quadratic shape function. For 2D element the shape of this matrix is following:

$$H(\xi) = \begin{pmatrix} N_1(\xi) & 0 & N_2(\xi) & 0 & N_3(\xi) & 0 \\ 0 & N_1(\xi) & 0 & N_2(\xi) & 0 & N_3(\xi) \end{pmatrix}. \tag{3.9}$$

As a result, we get

$$\Delta \boldsymbol{u}(\xi) = H(\xi) \Phi \boldsymbol{d}_N = B(\xi) \boldsymbol{d}_N, \tag{3.10}$$

where $B(\xi)$ has a dimension 2x12 and $\Delta \boldsymbol{u}(\xi)$ 2x1, thereby describing the continuous displacement field in both direction within the element. For large deformations, the element requires a local coordinate system to compute local deformations in normal and tangential directions. It leads to use the middle points of two element faces. If the coordinates of the initial configuration are given by the vector $\mathbf{x}_N$ and the deformation state is defined by the vector $\boldsymbol{d}_N$, the reference surface coordinates $\mathbf{x}_N^R$ are computed by linear interpolation between the top and bottom nodes in their deformed state:

$$\mathbf{x}_N^R = \frac{1}{2}(I_{6x6} \mid I_{6x6})(\mathbf{x}_N + \boldsymbol{d}_N). \tag{3.11}$$

The coordinates of the specific point are derived analogically such as in Eq. 3.8:

$$\mathbf{x}^R(\xi) = \begin{pmatrix} x^R(\xi) \\ y^R(\xi) \end{pmatrix} = H(\xi) \mathbf{x}_N^R. \tag{3.12}$$

The differentiation of the vector of global coordinates with respect to local coordinates and dividing its norm we obtain the unit length vector $\boldsymbol{t}_1$. The vector $\boldsymbol{t}_n$ perpendicular to the vector $\boldsymbol{t}_1$ is derived by the same way:

$$\boldsymbol{t}_1 = \frac{1}{\|\frac{\partial \mathbf{X}^R}{\partial \xi}\|}(\frac{\partial x^R}{\partial \xi}, \frac{\partial y^R}{\partial \xi})^T. \tag{3.13}$$

The norm of the vector is given by the standard definition:

$$\|\frac{\partial \mathbf{x}^R}{\partial \xi}\| = \sqrt{(\frac{\partial x^R}{\partial \xi})^2 + (\frac{\partial y^R}{\partial \xi})^2}. \tag{3.14}$$

The vectors $\boldsymbol{t}_1$ and $\boldsymbol{t}_n$ represent the direction cosines of the local coordinates system to global one, thus defining transformation tensor Θ:

$$\Theta = [\boldsymbol{t}_1, \boldsymbol{t}_N]. \tag{3.15}$$

This relates the local and global displacements as follows:

$$\Delta \boldsymbol{u}_{loc} = \Theta^T \Delta \boldsymbol{u}. \tag{3.16}$$

Subsequently we can mark by symbol $\boldsymbol{t}_{loc}$ vector describing the bridging stress relates to the local relative displacement with help of the constitutive relation for interface (cohesive) element:

$$\boldsymbol{t}_{loc} = \begin{pmatrix} \sigma_1 \\ \sigma_N \end{pmatrix} = C_{loc}(\Delta \boldsymbol{u}_{loc})\Delta \boldsymbol{u}_{loc}. \tag{3.17}$$

The constitutive relation can be expressed by linear displacement for Δu or more complicated, where Δu contains the nonlinear dependence. Just then in this is the trick of good numerical construction and new finite element creation. Preferred procedure depends on the shape of the constitutive equation. In Eq. 3.4 we used the nonlinear equation; it means that we come out from the relation:

$$\boldsymbol{t}_{loc} = \begin{pmatrix} \sigma_1 \\ \sigma_N \end{pmatrix} = C_{loc}\Delta \boldsymbol{u}_{loc}^{-1/2}. \tag{3.18}$$

Matrix C_{loc} is a constant now and does not depend on the displacement. The element stiffness matrix and the vector of the right hand side nodal force must be generated for the users' subroutine UEL. detJ is the Jacobian defined by the transformation of the global coordinates to the element coordinates. Jacobian needs to be derived for each integration point; in our case the Eq. 3.4 give us the stability of the computation. The stiffness matrix K (12x12 for 2D, 48x48 for 3D) is defined:

$$K^{el} = -\frac{\partial \boldsymbol{f}_N^{el}}{\partial \boldsymbol{d}^{el}}, \tag{3.19}$$

where

$$\boldsymbol{f}_N^{el} = \int_{-1}^{1} B^T \Theta \boldsymbol{t}_{loc} \mathrm{det}\mathbf{J} d\xi. \tag{3.20}$$

With the derivation one can found:

$$K = -W \int_{-1}^{1} B^T \Theta D_{loc} \Theta^T B \det \mathbf{J} d\xi. \tag{3.21}$$

And the stiffness matrix D is defined:

$$D_{loc} = \frac{\partial \boldsymbol{t}_{loc}}{\partial \Delta \boldsymbol{u}_{loc}}. \tag{3.22}$$

Or using Eq. 3.17

$$D_{loc} = \frac{\partial C(\Delta \boldsymbol{u})}{\partial \Delta \boldsymbol{u}} \Delta \boldsymbol{u} + C(\Delta \boldsymbol{u}). \tag{3.23}$$

4. Main results. First material (A) used for the bridging stresses modelling was a commercially available SiC Nicalon fibre reinforced borosilicate glass matrix composite. Properties of the glass matrix, SiC fibres and composite were: Young's modulus 63, 198, 118 GPa, Poisson ratio 0.22, 0.20, 0.21, tensile strength 60, 2750, 600-700 MPa. The fracture toughness determined using the bodies with Chevron notch were 24.6 MPam$^{0.5}$. Experimentally determined values were calibrated and the final values are: $J_0 = 6200$ J/m^2 (experiment), $\Delta J_{SS} = 18500$ J/m^2(experiment and calibration), $u_0 = 0.1$ mm (the end of the traction-separation law experiment), $u_1 = 0.013$ mm (calibration), $\alpha = 1$ (tested in range $\langle 1, 5 \rangle$). The final shape for the bridging law is in Fig. 4.1.

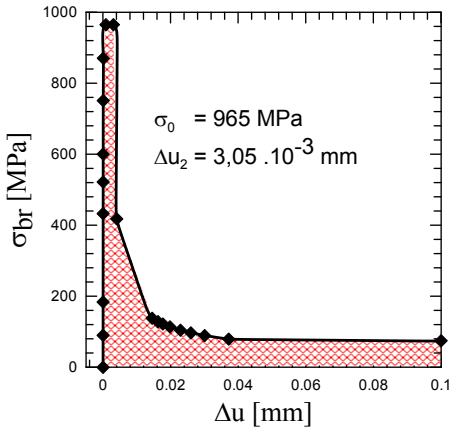

FIG. 4.1. *Final shape of the bridging law for material A*

Second material (B) used for the bridging stresses modelling was a Nextel 720 fibres reinforced fully pyrolyzed polysiloxane resin. Properties of the resin matrix, Nextel fibres and composite were: Young's modulus 70, 260, 180 GPa, Poisson ratio 0.22, 0.20, 0.21. The fracture toughness determined using the bodies with Chevron notch were 5 MPam$^{0.5}$. Experimentally determined values were calibrated and the final values are: $J_0 = 5010$ J/m^2 (experiment), $\Delta J_{SS} = 6050$ J/m^2 (experiment and calibration), $u_0 = 0.05$ mm (the end of the traction-separation law experiment), $u_1 = 0.01$ mm (calibration), $\alpha = 1$. The final shape for the bridging law is in Fig. 4.2.

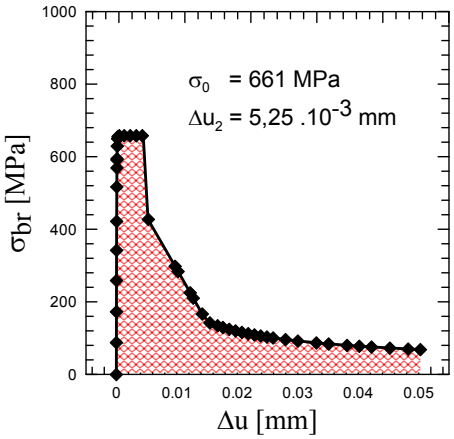

FIG. 4.2. *Final shape of the bridging law for material B*

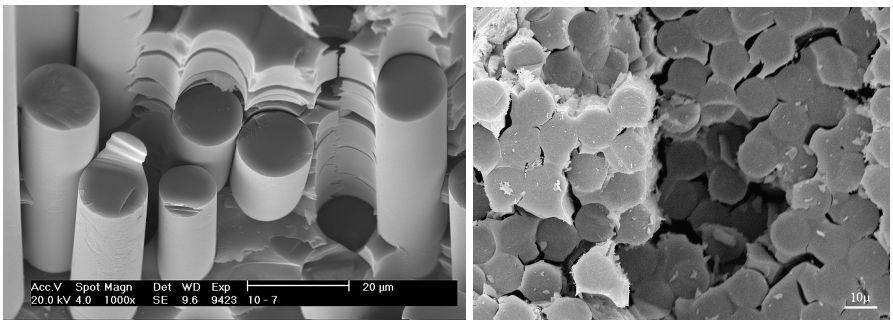

FIG. 4.3. *Fracture surface of material A and B*

Conclusions. The special finite element reflecting the bridging law for the long fibre composites has been created. This interface element was implemented into the standard Abaqus program using the user subroutine UEL. At the same time the experimental techniques needed for obtaining the experimental data were tested. The results can be characterized by following:

- The crack growth modelling for the long fibre composites is dependent on the bridging law shape. The stability of the interface element strongly depends on the first part of the bridging law, on the leading edge.
- The second key role is the mesh size, the application of the RVE seems to be necessary.
- Obtained results of the numerical modelling and running analysis of the microstructure enables combine the extended finite element method with cohesive zone method. The crack branching and crack creations modelling will be closer the material reality.

Vanishing elements for the crack growth simulation were tested and numerical stable shape of the traction separation law was suggested for SiC Nicalon fibres reinforced borosilicate glass matrix composite and Nextel 720 fibres reinforced fully pyrolyzed polysiloxane resin.

REFERENCES

[1] G. I. Barenblatt, Advances in Applied Mechanics. 7, (1962), pp. 55–129.
[2] D. S. Dugdale, Journal of the Mechanics and Physics of Solids, 8, (1960), pp. 100–104.
[3] A. Hillerborg, M. Modeer, P. E. Peterson, Cement and Concrete Research, 6, (1976), pp. 773–782.
[4] Z. H. Jin, C. T. Sun, International Journal of Solids and Structures, 43, (2006), pp. 1047–1060.
[5] J. Vala, *Scale Bridging in Diffusive Phase Transformation*, ALGORITMY 2009:18th Conference on Scientific Computing, Slovakia, (2009), pp. 362–371.
[6] O. Rabinowitch, Engineering Fracture Mechanics, 75, (2008), pp. 2842–2859.
[7] S. Shet, N. Chandra, Journal of Engng. Materials and Technology, 124, (2002), pp. 1–11.
[8] H. Li, N. Chandra, Int. J. of Plasticity, 19, (2003), pp. 849–882.
[9] M. Wiewer,R. Kabir, A. Cornec,K. H. Schwalbe, Engineering Fracture Mechanics, 74, Issue 16, (2007), pp. 2615–2638.
[10] E. Giner, N. Sukumar, et al., Engineering Fracture Mechanics, 76, (2009), pp. 347–368.
[11] N. Sukumar, J. H. Prvost,Int. Journal of Solids and Structures, 40, (2003), pp. 7513–7537.
[12] B. F. Sorensen, T. K. Jacobsen, Composites: Part A, 29 A, (1998), pp. 1443–1451.
[13] M. Kotoul, et al.: Theoretical and Applied Mechanics, 49, (2008), pp. 158–170.